Deceleration of Madden–Julian Oscillation Speed in NICAM AMIP-type Simulation Associated with Biases in the Walker Circulation Strength

Tamaki Suematsu[1], Hiroaki Miura[2], Chihiro Kodama[3], Daisuke Takasuka[3]

[1] Atmosphere and Ocean Research Institute, The University of Tokyo. [2] Graduate School of Science, The University of Tokyo. [3] Japan Agency for Marine-Earth Science and Technology

Corresponding author: Tamaki Suematsu (suematsu@aori.u-tokyo.ac.jp)

Key Points:

- The speed of Madden–Julian Oscillation (MJO) events in a 30-year global simulation with explicit cloud microphysics displayed a slow bias.
- The tendency of MJO to decelerate with the intensification of the Walker circulation was reproduced in the simulation.
- The slow bias of simulated MJO was attributed to overly strong western Walker cell, which was partially counteracted by El Niño events.

Abstract

The eastward movement speed of Madden–Julian Oscillation (MJO) events simulated in a 30-year simulation on a global cloud resolving model, nonhydrostatic icosahedral atmospheric model (NICAM), following the atmospheric model intercomparison project (AMIP) protocol, but with a slab ocean, was analyzed and compared with the observation. The simulation reproduced the observed tendency of the MJO to decelerate when they are embedded within stronger Walker circulation, intensified by background sea surface temperature states with larger zonal gradients between the warmer western Pacific and the cooler Indian ocean and eastern Pacific. However, the simulated MJO events displayed a slow bias and occurred disproportionately during El Niño events. These biases were associated with an overestimation of the western Walker circulation cell strength, which was partially counteracted during El Niño events. Our results highlight the importance of accurately reproducing the mean atmospheric circulation for the realistic reproduction of MJO in long term simulations.

Plain Language Summary

The characteristics of the eastward movement of the Madden-Julian Oscillation (MJO), which is the dominant mode of sub-seasonal variability in the tropical atmosphere, reproduced in a 30-year simulation on an atmospheric model with explicit cloud processes was analyzed. It was found that the simulation was able to reproduce the observed characteristic of the MJO to slow as the large-scale background zonal circulation in the tropics intensifies. However, the simulated MJO displayed a slow bias and occurred too frequently during El Niño events. This was associated with the influence of the El Niño counteracting the biases in the background zonal circulation. The results of the study emphasize the importance of accurately simulating the mean

atmospheric states for realistic simulation of the MJO in long-term simulations.

1 Introduction

The Madden–Julian Oscillation (MJO) (Madden & Julian, 1971) is the predominant intraseasonal variability in the tropics that is characterized by the slow eastward movement of the convective region, from the equatorial Indian Ocean (IO) to the western Pacific (WP). Far reaching influence of the MJO on the global weather patterns (Roxy et al., 2019; Zhang, 2013) and its potential as a source for predictability in extended-range forecasts (Tseng et al., 2020), makes them a particularly important phenomenon to successfully simulate. However, the realistic simulation of the MJO remains difficult for many state-of-the-art general circulation models (Ahn et al., 2017, 2020; Jiang et al., 2015; H. Kim et al., 2018). This difficulty has been associated with its high sensitivity to model representation of convective processes (Hannah & Maloney, 2011; Holloway et al., 2013), which are large sources of uncertainty in atmospheric simulations (Randall et al., 2003; Stevens & Bony, 2013).

The problem of simulating the MJO can be classified into the problem of hindcasting an MJO event as an initial value problem, and to the problem of simulating the MJO as an internal variability of the model reproduced atmosphere. Cloud-resolving models (CRM) with explicit formulations of cloud microphysics, have demonstrated their usefulness for hindcasting MJOs in sub-seasonal simulations (Holloway et al., 2013; Miura et al., 2007; Miyakawa et al., 2014). However, the high computational cost of CRMs hinders the investigation of the latter problem through conducting long-term ($\geq$ *O(10)* years) simulations.

The first ever multi-decadal simulation with explicit cloud microphysics was conducted by Kodama et al. (2015, hereafter K15) on the nonhydrostatic icosahedral atmospheric model (NICAM; Tomita & Satoh, 2004) following an atmospheric model intercomparison project

(AMIP) protocol (Gates, 1992), but with a slab ocean model. While the basic statistical properties of the MJO signals in this AMIP-type NICAM simulation (NICAM-AMIP simulation) have been investigated (Kikuchi et al., 2017; K15), the characteristics of the individual MJO events and their relationship with the model reproduced mean states have not been investigated.

The eastward movement of the MJO has been indicated to be strongly influenced by the background states of the sea surface temperatures (SST) in both observations (Suematsu & Miura, 2022, hereafter SM22; Wang et al., 2019; Wei & Ren, 2019) and long-term simulations (Chen et al., 2022; Klingaman & Demott, 2020). SM22 revealed that MJO events tend to decelerate when they are embedded within a strong Walker circulation, intensified by background SST states with large zonal SST gradients between the warmer WP and the cooler IO and eastern Pacific (EP). In this study we investigate the reproducibility of this relationship between the MJO speeds and the background states in the NICAM-AMIP simulation.

2 Data

2.1 NICAM-AMIP simulation

We analyzed data from the 30-year integration from NICAM-AMIP simulation from 1 June 1978 to 6 January 2009 (K15). The experiment was run with explicit formulation of cloud microphysics (Tomita, 2008), with approximately 14 km horizontal mesh, and 38 vertical layers with the model top at approximately 40 km. The initial atmospheric conditions were obtained from the European Centre for Medium-Range Weather Forecasts Reanalysis-40 (Uppala et al., 2005). The initial land condition was acquired from climatology of a 5-year NICAM simulation at 220 km mesh to reduce the initial shock. A 15 m mixed layer slab ocean model, nudged to SST from the Hadley Centre sea ice and SST dataset version 1 (Rayner et al., 2003), with a

relaxation time of 7 days, was coupled with the model. Further details on the experiment have been documented by K15. We examined daily averages of model outputs that were regridded to a resolution of 2.5° × 2.5° to match the observational data for comparability.

2.1 Observation and reanalysis

To analyze the observed MJO, we employed interpolated outgoing longwave radiation (OLR; Liebmann & Smith, 1996) data from the National Oceanic and Atmospheric Administration (NOAA), and the daily data of lower level (850 hPa) and upper level (200 hPa) zonal wind (U) velocities from the National Centers for Environmental Prediction-Department of Energy Reanalysis 2 (NCEP-DOE R2; Kanamitsu et al., 2002). Skin temperature from NCEP-DOE R2 was also used to analyze the surface mean states. The SST data were obtained from the NOAA Optimum Interpolated SST version 2 (Reynolds et al., 2002) for the period from 1 January 1982 to 31 December 2016. The resolution of SST was reduced to 2.5° × 2.5°. We refer to both the observational and reanalysis data as observations for brevity.

3 Methodologies

3.1 MJO detection

The MJO events in both the NICAM-AMIP simulation and observations were identified from time sequences that projected on to the real-time multivariate MJO (RMM) index (Wheeler & Hendon, 2004) from phase 2 to phase 7, while satisfying the following conditions employed by Suematsu and Miura (2018): 1) Phases do not skip forward nor recede backward by more than one phase. 2) The average amplitude is greater than the critical value of 0.8 (= A_c). 3) Period of consecutive days with amplitude below A_c is less than 15 days. 4) Transition from phase 2 to

phase 7 requires between 20 and 90 days.

Calculation of the RMM index followed the procedure of Wheeler and Hendon (2004) except for replacing their procedure to remove the signals of seasonal cycle and longer timescales to the removal of the long-term trend and the application of 20-120 day Lanczos band-pass filter (Duchon, 1979) with 241 symmetric weights. The RMM index sequence of the NICAM-AMIP data was calculated by projecting the simulated data on to eigenvectors of the observational data and by normalizing it using the standard deviations of the projections. MJO events detected by the above method that initiated and terminated between November and April were defined as boreal winter MJO events and were analyzed in this study.

3.2 MJO speed estimation

The MJO speeds were estimated following the procedure of SM22. Estimates were made by tracking daily the longitudes at which the 15°S–15°N meridionally averaged OLR anomaly took the minimum value. The tracking was conducted in the restricted longitude ranges of 50°E–120°E for phases 2 and 3, 50°E–150°E for phase 4, 100°E–150°W for phase 5, and 120°E–150°W for phases 6 and 7. The entire longitude ranges (50°E–150°W) were searched on days when the RMM amplitude dropped below A_c. The speed of an MJO event was estimated as a regression coefficient using the dates and longitudes of the tracked minimum OLR anomaly.

To confirm the consistency between the MJO speeds estimated from the tracked OLR anomalies in real-space and the trajectory of the MJO events on the RMM phase space, a condition was imposed to ensure that the estimated speeds displayed a linear relationship with the mean angular velocities in the RMM phase space. This was achieved by selecting MJO events that were distributed within 1.5 standard deviation from the regression line between the

132 angular velocities and MJO speeds. The same regression line and standard deviation derived
133 from observations were applied to make selections from the simulated MJO events. Angular
134 velocities were defined as the difference in polar angles between the last day of phase 7 and the
135 first day of phase 2 divided by the number of days between the two. The polar angles were
136 measured from the polar axis in the RMM1 axis in the negative direction.
137
138 **4 Results**
139 **4.1 Basic statistics of detected MJO events**
140 Using the above MJO detection and speed estimation method, 31 MJO events were
141 detected in the NICAM-AMIP simulation between the boreal winters of 1978–1979 and 2007–
142 2008, whereof eastward movement speeds were estimated for 21 events. From observations, 60
143 events were detected between the boreal winters of 1982–1983 and 2015–2016, whereof speeds
144 were estimated for 53 events. The number of MJO events per year in the NICAM-AMIP
145 simulation (1.0 events/year) was underestimated by a factor of 0.56 compared to that observed
146 (1.8 events/year).
147 The frequencies of MJO events in the NICAM-AMIP simulation and observations,
148 categorized by their movement speeds rounded to the nearest integer in m s^{-1}, are shown in
149 Figures 1a and 1b, respectively. The figures indicate that the simulated MJO tended to move
150 slower with smaller variations in their movement speeds compared to observations. The mean
151 speeds were 3.6 m s^{-1} and 4.4 m s^{-1} for the NICAM-AMIP simulation and observations,
152 respectively. These results are consistent with those of Kikuchi et al. (2017).
153 The slow bias of the simulated MJO was consistent with the mean durations of the events,
154 which were 45.0 and 36.2 days for the NICAM-AMIP simulation and observations, respectively.

Decompositions of the mean durations by the RMM phases are shown in Figures 1c and 1d. Days when the RMM amplitude was below A_c were grouped as days with low RMM amplitude. In all phases, mean durations were longer for the NICAM-AMIP simulation than those for observations. The mean relative contributions from each RMM phase to the lifetime of MJO events were remarkably similar. This signified that the deceleration and extended durations of the MJO events in the NICAM-AMIP simulation resulted from longer persistence of convection over all phases of the MJO and were not caused by a disproportionate stagnation of convection nor weakening of the MJO signal over any of the regions from IO to WP.

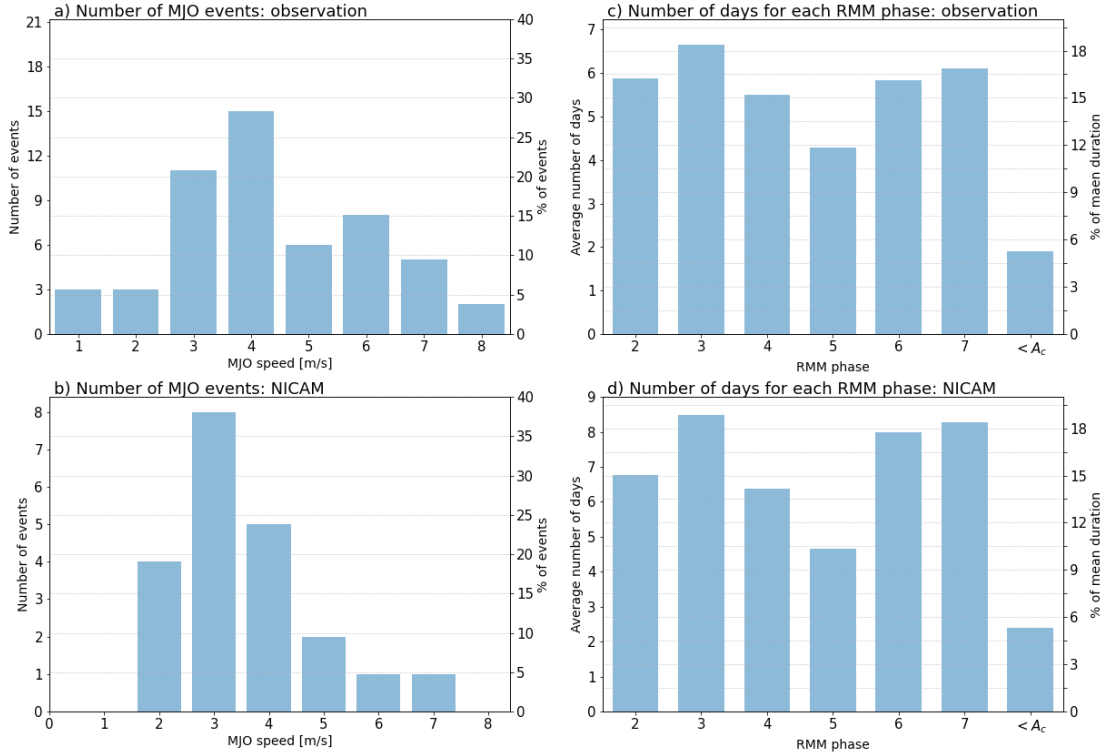

Figure 1. (a and b) Number of MJO events binned by their speeds rounded to the nearest integer in m s^{-1}, (c and d)and average number of days in each RMM phase in an MJO event for observations (a and c) and NICAM-AMIP simulation (b and d). The ordinates are adjusted so that the same heights in the histograms represent equal percentages of events in (a) and (b), and

mean durations in (c) and (d).

4.2 Relationship between MJO speeds and background fields

Variations and biases in the simulated MJO speeds were associated with slow changes in the SST fields, which serve as the background SST states for MJO. These were examined and compared with observations. Figures 2a (adapted from SM22) and 2b show the observed and simulated correlation patterns between the background SST on the day of the MJO initiation and the MJO speeds, respectively. Because the longest MJO event in our analysis was 67 days, the background SST was defined as the 90-day low pass filtered SST using a Lanczos filter (Duchon 1979) with 241 symmetric weights. Figures 2a and 2b indicate that the NICAM-AMIP simulation reproduced the observed tendency of the MJO to accelerate under El Niño, which reduces the SST gradients between the IO, WP, and EP (Nishimoto & Shiotani, 2013; Pohl & Matthews, 2007; SM2022; Wang et al., 2019; Wei & Ren, 2019). However, the correlation over the WP was weak for the NICAM-AMIP simulation, and it appears that the MJO speeds in the simulation were modulated mainly by the SST variations over the IO and EP.

As the thermally direct cells of Walker circulation are modulated by the zonal gradients of the background SST (Bjerknes, 1969), we further examined the relationship between the simulated MJO speeds and the strengths of the Walker circulation that they occurred in. Figures 2c (adapted from SM22) and 2d show the correlation pattern of the 5°S–5°N averaged background U with the initiation of the MJO events, for the observations and NICAM-AMIP simulation, respectively. The background circulation was defined using the same filter for defining the background SST.

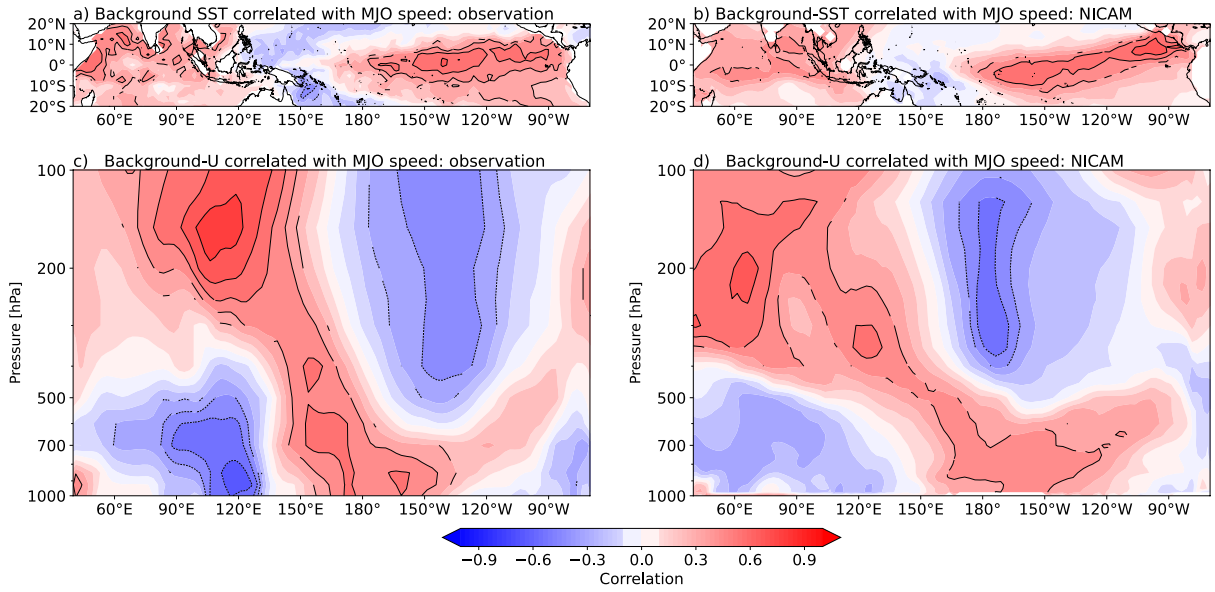

Figure 2. (a and b) Correlation pattern between MJO speed and background SST, and (c and d) 5°S–5°N averaged U, at the initiation of MJO events for observations (a and c) and NICAM-AMIP simulation (b and d). The contours indicate the location where the correlations are significant at a 95% confidence level.

As shown by SM22, MJO tended to slow under a strong Walker circulation. The general characteristics of the correlation pattern of the NICAM-AMIP simulation were consistent with the observations. However, the pattern was distorted as the correlation over the IO was strongest over the western IO rather than over the Maritime Continent, as in observations. This indicates that the acceleration of the upper-level (300 –200 hPa) easterlies over the western IO rather than over the Maritime Continent is associated with the deceleration of the MJO speed. Moreover, the negative correlation of upper-level U over the central Pacific was confined in a narrow zonal range near the date line for the NICAM-AMIP simulation, while it extended beyond 120°W in observations. Therefore, while the NICAM-AMIP simulation was able to

reproduce the tendency of the MJO to decelerate under a strong western Walker circulation cell, the distorted correlation pattern of Figure 2d implies that the Walker circulation may be misrepresented in the NICAM-AMIP simulation. Further discussion on the biases in the simulated Walker circulation and its possible influence on the simulated MJO is provided in subsection 4.4.

4.3 Enhancement of simulated MJO by ENSO

In the previous subsection, we only inferred the correlations and did not consider any systematic biases in the simulation with regards to the conditions that may have enhanced or suppressed the reproducibility of the MJO. Here, we examine the SST conditions that MJO events in the NICAM-AMIP simulation occurred in, and how they compare with observations.

Preceding studies have indicated that zonal SST gradient in which SST increases towards the WP from both the IO and EP enhances and modulates the eastward movement of the MJO in observations (Hirata et al., 2013; Suematsu & Miura, 2018, 2022) and simulations (Chen et al., 2022; H.-M. Kim et al., 2016; Klingaman & Demott, 2020; Miura et al., 2009, 2015). Following SM22, we examined the occurrences of MJO events by an index of zonal SST gradient defined as:

$$\boldsymbol{\Delta}\mathrm{SST} = \mathrm{SST_{WP}} - \frac{\mathrm{SST_{IO}} + \mathrm{SST_{EP}}}{\mathbf{2}} \#(\mathbf{1})$$

where $\mathrm{SST_{WP}}$, $\mathrm{SST_{IO}}$, and $\mathrm{SST_{EP}}$ are the area-averaged SST over WP (15°S–15°N, 140°E–160°E), IO (15°S–15°N, 60°E–100°E), and EP (15°S–15°N, 160°W–120°W), respectively.

The scatter plots displaying the speed of MJO events and **Δ**SST averaged over 10 days before initiation are shown in Figures 3a (adapted from SM22) and 3b for observations and the

NICAM-AMIP simulation, respectively. MJO events were found to be negatively correlated with **Δ**SST for both the observations (-0.66) and simulation (-0.51). However, MJO events in the NICAM-AMIP simulation occurred at lower values of **Δ**SST than those in observations, and a third of the detected events occurred under negative **Δ**SST conditions.

The interannual variability of the SST has been indicated to be the primary cause for changes in **Δ**SST (SM22). Thus, we examined the frequency of occurrence of MJO events by the strength of the El Niño Southern Oscillation (ENSO), which is the dominant source of interannual SST variability. We employ the Ocean Niño Index (ONI; Trenberth, 1997), calculated as 91 day running means of SST anomalies averaged over the Niño 3.4 region (5°S–5°N, 170°W–120°W), to evaluate the ENSO phases. Episodes of El Niño and La Niña are defined as periods when the index is > 0.5 K and < -0.5 K, respectively.

Figures 3c and 3d show the frequency of MJO events by the ONI, averaged over their lifetimes for observations and the NICAM-AMIP simulation, respectively. MJO events in the observation occurred nearly evenly among the ENSO phases, with slightly more (6%) MJO events during La Niña. However, the reproducibility of the MJO events in the NICAM-AMIP simulation was highly sensitive to the ENSO phase; MJO events occurred more than three times as frequently during El Niño (ONI > 0.5 K, 33%) than during La Niña (ONI < -0.5 K, 10%), and no MJO events occurred under moderate and strong La Niña conditions (ONI < -1.0 K).

In the NICAM-AMIP simulation, biases in SST are expected to be small because it was nudged to observation. Thus, we investigate the biases in the mean states of the atmosphere and land surfaces for providing a coherent explanation of the relationship between MJO and SST conditions within the NICAM-AMIP simulation.

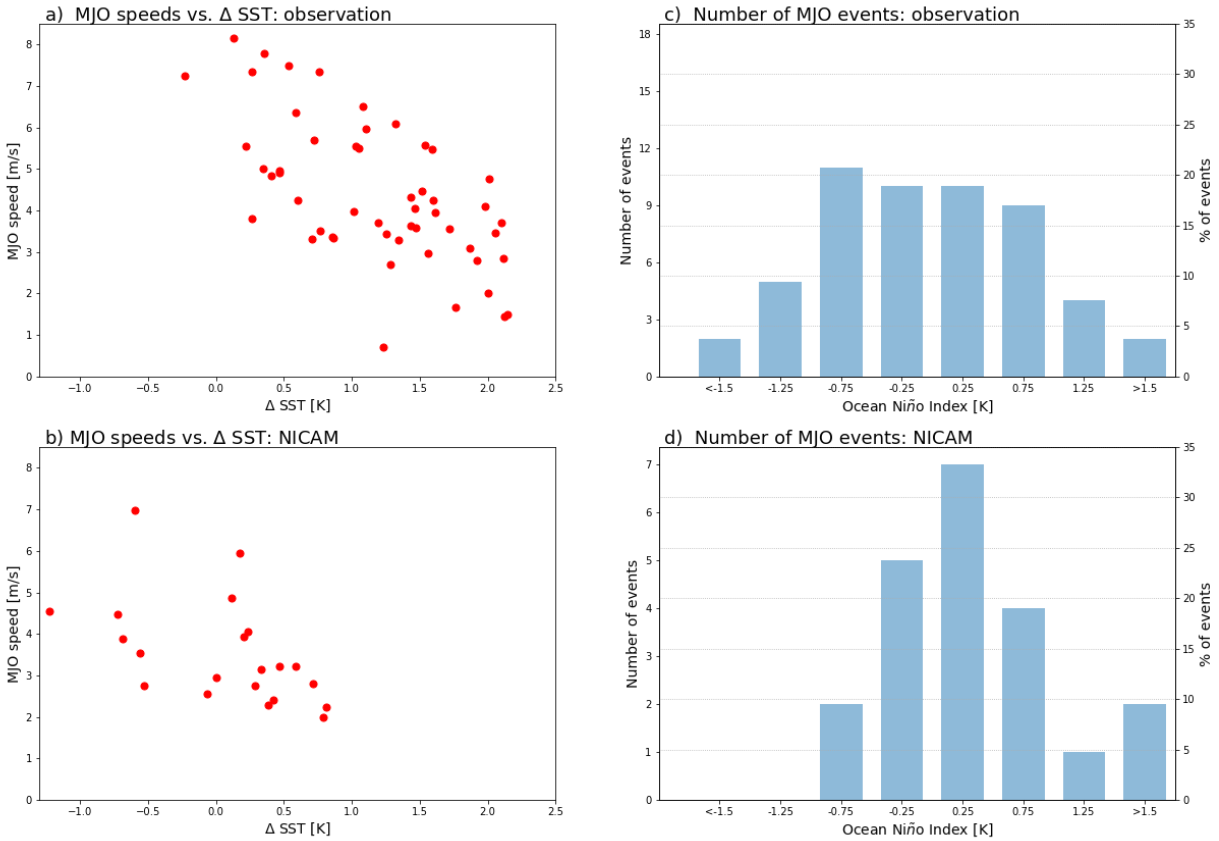

Figure 3. (a and b) Scatter plots of MJO speed [m s^{-1}] and **Δ** SST [K] averaged over 10 days before the initiation of MJO, and (c and d) histograms of the number of MJO events binned by the mean values of ONI during their lifetimes at 0.5 K intervals for observations (a and c) and the NICAM-AMIP simulation (b and d). The ordinates in (c) and (d) are adjusted so that the same heights in the histograms represent equal percentages of events.

4.4 Biases in the mean states

The mean states of the zonal circulation were compared between observations and the NICAM-AMIP simulation. Figures 4a and 4b show the November–April climatology of 5°S–5°N meridionally averaged U for the observations and NICAM-AMIP simulation, respectively.

261 The figures highlight that the NICAM-AMIP simulation reproduced a mean state with an overly
262 strong western Walker circulation cell. The simulated western Walker cell extended beyond
263 60°E, where the western edge of the western cell in the observation was approximately located,
264 and the strength of the upper level (200 hPa–100 hPa) easterlies and low level (700 hPa)
265 westerlies from western IO (approximately 40°E) to the date line, were overestimated. In
266 contrast, the strength of the eastern Walker cell in the NICAM-AMIP simulation was
267 underestimated and was confined to a zonally narrower region between the date line and 120°W,
268 whereas it extended to 90°W for observations.

269 To determine a possible cause for the biases in the strengths of the Walker circulation, the
270 mean states of skin temperature were analyzed (Figures 4c and 4d). Comparisons of the
271 climatological November–April mean skin temperature revealed that there was a large high skin
272 temperature bias over northern Australia in the NICAM-AMIP simulation. Skin temperature was
273 also warmer by 1–2 K in the NICAM-AMIP simulation from IO to WP, which may be due to the
274 bias in longwave cloud radiative forcing shown by K15. The overall pattern of the skin
275 temperature biases was consistent with the intensified Walker circulation over IO to the WP in
276 the NICAM-AMIP simulation.

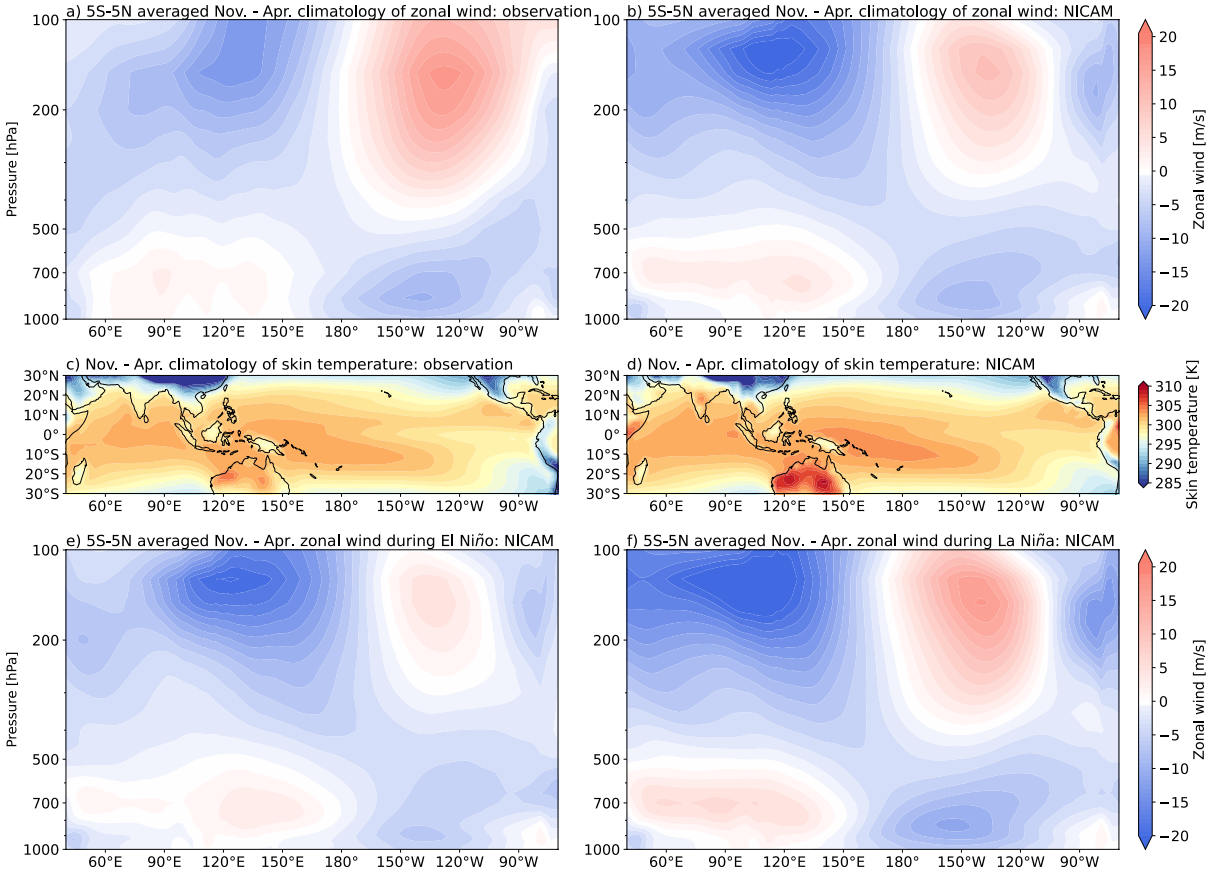

277

278 **Figure 4.** November to April climatology of (a and b) 5°S–5°N averaged U [m s^{-1}], and (c and d)
279 skin temperature [K] for observations (a and c) and NICAM-AMIP simulation (b and d). (e and
280 f) as in (a and b) but during El Niño (e) and La Niña (f) events in NICAM-AMIP simulation.

281

282 Slow changes in the zonal SST gradient caused by ENSO may counteract or enhance the
283 biases in the skin temperature and the Walker circulation strength in the NICAM-AMIP
284 simulation. Figures 4e and 4f compare the November–April mean zonal circulation in the
285 NICAM-AMIP simulation during El Niño and La Niña, respectively. These figures show that
286 both sides of the Walker circulation cells were weakened and strengthened during El Niño and
287 La Niña, respectively. Thus, the overly strong bias of the western Walker cell decreased during
288 El Niño and increased during La Niña. Additionally, low level (approximately 850 hPa)

289 westerlies from the IO extended to the date line in the NICAM-AMIP simulation during El Niño,
290 which may be associated with the zonal extension of the MJO convective region. MJO events
291 were spuriously enhanced in the NICAM-AMIP simulation during El Niño, when the simulated
292 background circulation of the convectively active region was closer to the observed
293 climatological state. The simulated western Walker cell during El Niño remained stronger than
294 the observed November–April climatology, which may be associated with the slower mean MJO
295 speed in the NICAM-AMIP simulation.
296
297 **5 Summary and Discussion**
298 Simulation of the MJO has long been recognized as a challenging problem. The
299 elimination of convective parameterization in CRM has improved the reproducibility of the MJO
300 as an initial value problem (e.g., Miura et al. 2007; Miyakawa et al. 2014). However, there is
301 limited analysis of MJO events reproduced as internal variabilities of the modelled atmosphere
302 by global CRMs (Kikuchi et al. 2017; K15). In this study, we detected MJO events and analyzed
303 their statistical properties reproduced in a 30-year NICAM-AMIP simulation (K15). The
304 relationship between the variability of MJO speeds, and the background SST and zonal
305 circulation states, identified in a recent study by SM22, was the focus of our analyses.
306 Individual MJO events were identified in the NICAM-AMIP simulation and compared
307 with observations. It was found that the NICAM-AMIP simulation tended to reproduce
308 approximately half the number of MJO events in a given period compared to observations. The
309 simulated MJO events tended to be slower and lasted longer than those observed, indicating that
310 the smaller number of MJO events was partially compensated by longer lifetimes, with regards
311 to the overall activity of the simulated intraseasonal variability.

312 The observed MJO speeds decelerate with the intensification of the Walker circulation
313 cell owing to increased zonal SST gradients between the warmer WP and cooler IO and EP
314 (SM22). The relationship was reproduced well in the NICAM-AMIP simulation; the simulated
315 MJO speed highlighted a clear negative correlation between the **Δ**SST and the strength of Walker
316 circulation. However, detailed inspection of the SST distributions at which MJO events occurred
317 revealed that simulated MJO occurred during periods when zonal SST gradient was much
318 smaller than for those observed. MJO events were spuriously enhanced and suppressed during El
319 Niño and La Niña events, respectively, in the NICAM-AMIP simulation.

320 Previous studies have also identified model specific enhancements of the MJO by El
321 Niño, associated with moisture fluxes (Chen et al., 2022) and spurious corrections of cold SST
322 biases (Klingaman & Demott, 2020). Biases in the atmospheric mean states were examined for
323 explaining the disproportionate occurrence of MJO events during El Niño. It was revealed that
324 the NICAM-AMIP simulation produced mean states with an overly strong western Walker
325 circulation cell, where the convectively active region of the MJO coincides. El Niño alleviated
326 this model bias towards more realistic background circulation states from the IO to WP, which
327 enabled reproduction of MJO events in the simulation.

328 Questions remain on whether the dynamic processes that modulate the effects of the
329 Walker circulation strength on the MJO speed were realistically reproduced in the NICAM-
330 AMIP simulation. The variability in the composition of convective systems within the MJO
331 envelope should be investigated in a future study to address this uncertainty. For example,
332 whether the observed MJO initiation processes involving interaction between the mixed Rossby-
333 gravity waves and the Walker circulation (Takasuka et al., 2021) was simulated, is of particular
334 interest. It is also of interest to clarify how the inclusion of air–sea interactions in the fully ocean

coupled version of NICAM (Miyakawa et al., 2017) could affect the model mean states and the eastward movement of the MJO.

Acknowledgments

T. Suematsu was supported by JSPS KAKENHI Grants 16J07769, 21K13991 and 20H05730. H. Miura was supported by JSPS KAKENHI 16H04048 and 20H05729. C. Kodama and D. Takasuka was supported by JSPS KAKENHI Grants 20H05728. The NICAM–AMIP simulation was performed on the K computer at the RIKEN R-CCS (Proposal numbers hp120279, hp130010, and hp140219).

Open Research

NOAA-OLR data are available online (https://psl.noaa.gov/data/gridded/data.interp_OLR.html); The NOAA OI SST V2 high-resolution dataset is available online at (https://psl.noaa.gov/data/gridded/data.noaa.oisst.v2.highres.html); NCEP-DOE reanalysis data are available online at (https://psl.noaa.gov/data/gridded/data.ncep.reanalysis2.html); and NICAM-AMIP simulation data used in this study are available online at (https://zenodo.org/record/6348628#.Yi6WgbhUtaR).

References

Ahn, M. S., Kim, D., Kang, D., Lee, J., Sperber, K. R., Gleckler, P. J., Jiang, X., Ham, Y. G., & Kim, H. (2020). MJO Propagation Across the Maritime Continent: Are CMIP6 Models Better Than CMIP5 Models? *Geophysical Research Letters*, *47*(11), e2020GL087250. https://doi.org/10.1029/2020GL087250

Ahn, M. S., Kim, D., Sperber, K. R., Kang, I. S., Maloney, E., Waliser, D., & Hendon, H. (2017). MJO simulation in CMIP5 climate models: MJO skill metrics and process-oriented diagnosis. *Climate Dynamics*, *49*(11–12), 4023–4045. https://doi.org/10.1007/S00382-017-3558-4/FIGURES/10

Bjerknes, J. (1969). ATMOSPHERIC TELECONNECTIONS FROM THE EQUATORIAL PACIFIC. *Monthly Weather Review*, *97*(3), 163–172. https://doi.org/10.1175/1520-

0493(1969)097<0163:ATFTEP>2.3.CO;2

Chen, G., Ling, J., Zhang, Y., Wang, X., & Li, C. (2022). MJO Propagation over the Indian Ocean and Western Pacific in CMIP5 Models: Roles of Background States. *Journal of Climate*, *35*(3), 955–973. https://doi.org/10.1175/JCLI-D-21-0255.1

Duchon, C. E. (1979). Lanczos Filtering in One and Two Dimensions. *Journal of Applied Meteorology*, *18*(8), 1016–1022. https://doi.org/10.1175/1520-0450(1979)018<1016:LFIOAT>2.0.CO;2

Gates, W. L. (1992). AMIP: The Atmospheric Model Intercomparison Project. *Bulletin of the American Meteorological Society*, *73*(12), 1962–1970. https://doi.org/10.1175/1520-0477(1992)073<1962:ATAMIP>2.0.CO;2

Hannah, W. M., & Maloney, E. D. (2011). The role of moisture-convection feedbacks in simulating the Madden-Julian oscillation. *Journal of Climate*, *24*(11), 2754–2770. https://doi.org/10.1175/2011JCLI3803.1

Hirata, F. E., Webster, P. J., & Toma, V. E. (2013). Distinct manifestations of austral summer tropical intraseasonal oscillations. *Geophysical Research Letters*, *40*(12), 3337–3341. https://doi.org/10.1002/grl.50632

Holloway, C. E., Woolnough, S. J., & Lister, G. M. S. (2013). The Effects of Explicit versus Parameterized Convection on the MJO in a Large-Domain High-Resolution Tropical Case Study. Part I: Characterization of Large-Scale Organization and Propagation. *Journal of the Atmospheric Sciences*, *70*(5), 1342–1369. https://doi.org/10.1175/JAS-D-12-0227.1

Jiang, X., Waliser, D. E., Xavier, P. K., Petch, J., Klingaman, N. P., Woolnough, S. J., Guan, B., Bellon, G., Crueger, T., DeMott, C., Hannay, C., Lin, H., Hu, W., Kim, D., Lappen, C.-L., Lu, M.-M., Ma, H.-Y., Miyakawa, T., Ridout, J. A., … Zhu, H. (2015). Vertical structure and physical processes of the Madden-Julian oscillation: Exploring key model physics in climate simulations. *Journal of Geophysical Research: Atmospheres*, *120*(10), 4718–4748. https://doi.org/10.1002/2014JD022375

Kanamitsu, M., Ebisuzaki, W., Woollen, J., Yang, S.-K., Hnilo, J. J., Fiorino, M., Potter, G. L., Kanamitsu, M., Ebisuzaki, W., Woollen, J., Yang, S.-K., Hnilo, J. J., Fiorino, M., & Potter, G. L. (2002). NCEP–DOE AMIP-II Reanalysis (R-2). *Bulletin of the American Meteorological Society*, *83*(11), 1631–1644. https://doi.org/10.1175/BAMS-83-11-1631

Kikuchi, K., Kodama, C., Nasuno, T., Nakano, M., Miura, H., Satoh, M., Noda, A. T., & Yamada, Y. (2017). Tropical intraseasonal oscillation simulated in an AMIP-type experiment by NICAM. *Climate Dynamics*, *48*(7–8), 2507–2528. https://doi.org/10.1007/s00382-016-3219-z

Kim, H.-M., Kim, D., Vitart, F., Toma, V. E., Kug, J.-S., & Webster, P. J. (2016). MJO Propagation across the Maritime Continent in the ECMWF Ensemble Prediction System. *Journal of Climate*, *29*(11), 3973–3988. https://doi.org/10.1175/JCLI-D-15-0862.1

Kim, H., Vitart, F., & Waliser, D. E. (2018). Prediction of the Madden–Julian Oscillation: A Review. *Journal of Climate*, *31*(23), 9425–9443. https://doi.org/10.1175/JCLI-D-18-0210.1

Klingaman, N. P., & Demott, C. A. (2020). Mean State Biases and Interannual Variability Affect Perceived Sensitivities of the Madden-Julian Oscillation to Air-Sea Coupling. *Journal of*

Advances in Modeling Earth Systems, *12*(2), e2019MS001799. https://doi.org/10.1029/2019MS001799

Kodama, C., Yamada, Y., Noda, A. T., Kikuchi, K., Kajikawa, Y., Nasuno, T., Tomita, T., Yamaura, T., Takahashi, H. G., Hara, M., Kawatani, Y., Satoh, M., & Sugi, M. (2015). A 20-Year Climatology of a NICAM AMIP-Type Simulation. *Journal of the Meteorological Society of Japan. Ser. II*, *93*(4), 393–424. https://doi.org/10.2151/jmsj.2015-024

Kodama, C., & T., Suematsu, (2022). NICAM AMIP-type simulation data for the article "Deceleration of Madden–Julian Oscillation Speed in NICAM AMIP-type Simulation Associated with Biases in the Walker Circulation Strength". Zenodo. https://doi.org/10.5281/zenodo.6348628

Liebmann, B., & Smith, C. (1996). Description of a complete (interpolated) outgoing longwave radiation dataset. *Bull. Amer. Met. Soc.*, *77*, 1275–1277.

Madden, R. A., & Julian, P. R. (1971). Detection of a 40–50 Day Oscillation in the Zonal Wind in the Tropical Pacific. *Journal of the Atmospheric Sciences*, *28*(5), 702–708. https://doi.org/10.1175/1520-0469(1971)028<0702:DOADOI>2.0.CO;2

Miura, H., Satoh, M., & Katsumata, M. (2009). Spontaneous onset of a Madden-Julian oscillation event in a cloud-system-resolving simulation. *Geophysical Research Letters*, *36*(13), L13802. https://doi.org/10.1029/2009GL039056

Miura, H., Satoh, M., Nasuno, T., Noda, A. T., & Oouchi, K. (2007). A Madden-Julian Oscillation Event Realistically Simulated by a Global Cloud-Resolving Model. *Science*, *318*(5857), 1763–1765. https://doi.org/10.1126/science.1148443

Miura, H., Suematsu, T., & Nasuno, T. (2015). An Ensemble Hindcast of the Madden-Julian Oscillation during the CINDY2011/DYNAMO Field Campaign and Influence of Seasonal Variation of Sea Surface Temperature. *Journal of the Meteorological Society of Japan. Ser. II*, *93A*, 115–137. https://doi.org/10.2151/jmsj.2015-055

Miyakawa, T., Yashiro, H., Suzuki, T., Tatebe, H., & Satoh, M. (2017). A Madden-Julian Oscillation event remotely accelerates ocean upwelling to abruptly terminate the 1997/1998 super El Niño. *Geophysical Research Letters*, *44*(18), 9489–9495. https://doi.org/10.1002/2017GL074683

Miyakawa, Tomoki, Satoh, M., Miura, H., Tomita, H., Yashiro, H., Noda, A. T., Yamada, Y., Kodama, C., Kimoto, M., & Yoneyama, K. (2014). Madden–Julian Oscillation prediction skill of a new-generation global model demonstrated using a supercomputer. *Nature Communications*, *5*. https://doi.org/10.1038/ncomms4769

Nishimoto, E., & Shiotani, M. (2013). Intraseasonal variations in the tropical tropopause temperature revealed by cluster analysis of convective activity. *Journal of Geophysical Research: Atmospheres*, *118*(9), 3545–3556. https://doi.org/10.1002/jgrd.50281

Pohl, B., & Matthews, A. J. (2007). Observed Changes in the Lifetime and Amplitude of the Madden–Julian Oscillation Associated with Interannual ENSO Sea Surface Temperature Anomalies. *Journal of Climate*, *20*(11), 2659–2674. https://doi.org/10.1175/JCLI4230.1

Randall, D., Khairoutdinov, M., Arakawa, A., & Grabowski, W. (2003). Breaking the Cloud Parameterization Deadlock. *Bulletin of the American Meteorological Society*, *84*(11), 1547–

1564. https://doi.org/10.1175/BAMS-84-11-1547

Rayner, N. A., Parker, D. E., Horton, E. B., Folland, C. K., Alexander, L. V., Rowell, D. P., Kent, E. C., & Kaplan, A. (2003). Global analyses of sea surface temperature, sea ice, and night marine air temperature since the late nineteenth century. *Journal of Geophysical Research*, *108*(D14), 4407. https://doi.org/10.1029/2002JD002670

Reynolds, R. W., Rayner, N. A., Smith, T. M., Stokes, D. C., & Wang, W. (2002). An Improved In Situ and Satellite SST Analysis for Climate. *Journal of Climate*, *15*(13), 1609–1625. https://doi.org/10.1175/1520-0442(2002)015<1609:AIISAS>2.0.CO;2

Roxy, M. K., Dasgupta, P., McPhaden, M. J., Suematsu, T., Zhang, C., & Kim, D. (2019). Twofold expansion of the Indo-Pacific warm pool warps the MJO life cycle. *Nature*, *575*(7784), 647–651. https://doi.org/10.1038/s41586-019-1764-4

Stevens, B., & Bony, S. (2013). What Are Climate Models Missing? *Science*, *340*(6136), 1053–1054. https://doi.org/10.1126/SCIENCE.1237554

Suematsu, T., & Miura, H. (2018). Zonal SST Difference as a Potential Environmental Factor Supporting the Longevity of the Madden–Julian Oscillation. *Journal of Climate*, *31*(18), 7549–7564. https://doi.org/10.1175/JCLI-D-17-0822.1

Suematsu, T., & Miura, H. (2022). Changes in the Eastward Movement Speed of the Madden–Julian Oscillation with Fluctuation in the Walker Circulation. *Journal of Climate*, *35*(1), 211–225. https://doi.org/10.1175/JCLI-D-21-0269.1

Takasuka, D., Kohyama, T., Miura, H., & Suematsu, T. (2021). MJO Initiation Triggered by Amplification of Upper-Tropospheric Dry Mixed Rossby-Gravity Waves. *Geophysical Research Letters*, *48*(20), e2021GL094239. https://doi.org/10.1029/2021GL094239

Tomita, H. (2008). New Microphysical Schemes with Five and Six Categories by Diagnostic Generation of Cloud Ice. *Journal of the Meteorological Society of Japan. Ser. II*, *86A*, 121–142. https://doi.org/10.2151/JMSJ.86A.121

Tomita, H., & Satoh, M. (2004). A new dynamical framework of nonhydrostatic global model using the icosahedral grid. *Fluid Dynamics Research*, *34*(6), 357–400. https://doi.org/10.1016/j.fluiddyn.2004.03.003

Trenberth, K. E. (1997). The Definition of El Niño. *Bulletin of the American Meteorological Society*, *78*(12), 2771–2777. https://doi.org/10.1175/1520-0477(1997)078<2771:TDOENO>2.0.CO;2

Tseng, K. C., Barnes, E. A., & Maloney, E. (2020). The Importance of Past MJO Activity in Determining the Future State of the Midlatitude Circulation. *Journal of Climate*, *33*(6), 2131–2147. https://doi.org/10.1175/JCLI-D-19-0512.1

Uppala, S. M., Kållberg, P. W., Simmons, A. J., Andrae, U., da Costa Bechtold, V., Fiorino, M., Gibson, J. K., Haseler, J., Hernandez, A., Kelly, G. A., Li, X., Onogi, K., Saarinen, S., Sokka, N., Allan, R. P., Andersson, E., Arpe, K., Balmaseda, M. A., Beljaars, A. C. M., … Woollen, J. (2005). The ERA-40 re-analysis. *Quarterly Journal of the Royal Meteorological Society*, *131*(612), 2961–3012. https://doi.org/10.1256/QJ.04.176

Wang, B., Chen, G., & Liu, F. (2019). Diversity of the Madden-Julian Oscillation. *Science Advances*, *5*(7), eaax0220. https://doi.org/10.1126/sciadv.aax0220

Wei, Y., & Ren, H.-L. (2019). Modulation of ENSO on Fast and Slow MJO Modes during Boreal Winter. *Journal of Climate*, *32*(21), 7483–7506. https://doi.org/10.1175/JCLI-D-19-0013.1

Wheeler, M. C., & Hendon, H. H. (2004). An All-Season Real-Time Multivariate MJO Index: Development of an Index for Monitoring and Prediction. *Monthly Weather Review*, *132*(8), 1917–1932. https://doi.org/10.1175/1520-0493(2004)132<1917:AARMMI>2.0.CO;2

Zhang, C. (2013). Madden–Julian Oscillation: Bridging Weather and Climate. *Bulletin of the American Meteorological Society*, *94*(12), 1849–1870. https://doi.org/10.1175/BAMS-D-12-00026.1